Excerpt from the Proceedings of the 2011 COMSOL Conference in Stuttgart

Using Computational Multiphysics to Optimise Channel Design for a Novel PEM Fuel Cell Stack

Flora A. Daniels[1], Daniel J.L. Brett[*,1], Anthony R. Kucernak[2] and Cynthia Attingre[2]
[1]University College London, [2]Department of Chemistry, Imperial College London
*Corresponding author: University College London, Torrington Place, London, UK, WC1E 7JE, d.brett@ucl.ac.uk

Abstract: A three-dimensional mathematical model of a polymer electrolyte membrane (PEM) fuel cell using printed circuit board (PCB) current collectors with two different flow field designs is presented. The model takes into account species, momentum and heat transport phenomena within each fuel cell configuration. The purpose of the model is to evaluate the effect of flow field design on the operation of a fuel cell. The results of the model give a better understanding of important considerations such as water and heat management. The fully-coupled model shows that there is a strong link between flow field plate design and cell performance. Current and reactant species transport within the cell are governed by the flow field design and, consequently, have a non-uniform distribution within the porous layers. Improvements in the design and operation of the fuel cell are suggested based on model results.

Keywords: PEM fuel cell, fuel cell modelling, flow field design, CFD.

1. Introduction

PEM fuel cells are quickly becoming an attractive technology due to their ability to meet increasing energy demands in a cleaner, more efficient way compared to existing methods. Their ability to convert chemical energy, in the form of hydrogen and oxygen, into electrical current makes them a promising zero-carbon emission source of energy production. They are accessible to a variety of applications ranging from portable power solutions, transportation and stationary power due to their advantageous design flexibility and scalability.

The core of the PEM fuel cell consists of: the polymer electrolyte membrane, the electrodes and the gas diffusion layers (GDL), which form the membrane electrode assembly (MEA), and the mono- or bipolar plates, shown in Figure 1. Connecting multiples of these units in electrical series results in the formation of a stack.

The bipolar plate plays a key role in PEMFC operation: to collect and transport current produced by the MEA, to provide structural stability and to distribute reactants to the surfaces of the MEA. Extensive research has been completed on transport phenomena, flow field design and the effects of varying operating parameters (e.g. reactant flowrates, gas humidification) using these bipolar plates in fuel cell operation [1-8].

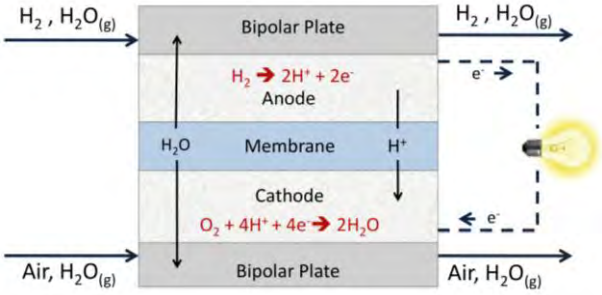

Figure 1. A schematic diagram of the key components of a PEM fuel cell and its operation.

Traditional bipolar plates are made of graphite or graphite composite materials. However, these plates tend to be bulky and expensive due to high manufacturing costs. Using PCBs in lieu of graphite materials for bipolar plates have significant potential as they are lightweight, can be easily manufactured for complex designs and are more cost effective.

Modelling provides a better understanding of the effects of PCB flow field design on the overall performance of the PEM fuel cell. Analysis of the key operating characteristics allow for optimization and selection of the most suitable design for the fuel cell unit. Consequently, modelling enables faster evaluation of candidate technologies in the design-to-manufacturing process.

2. Model Description

A three-dimensional, steady-state, non-isothermal, single-phase model was produced for current collectors with two different flow field designs shown in Figure 2. Each model consists of a 5 cm^2 active area of an MEA placed between two PCB current collectors with the same flow field design.

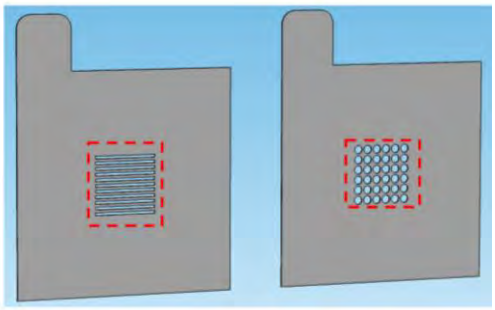

Figure 2. A three-dimensional representation of the parallel channel flow field plate (left) and the circular channel flow field plate (right). The active areas modeled are highlighted by the red dashed boxes.

Two designs were selected for investigation: a parallel and a circular channel flow field. The parallel flow field consists of 11 parallel channels with a channel and rib width of 1 mm each. The circular flow field consists of 36 circular channels with a diameter of 3 mm and cell pitch of 0.7 mm between each channel. Gases flow through a plenum area on the rear of the current collector.

In order to gain a better understanding of the fuel cell operation, each model takes into account key transport phenomena:

1. Multi-component diffusion through the porous gas diffusion and catalyst layers.
2. Convection of reactant gases across the gas channels.
3. Conduction of electrons through the gas diffusion and catalyst layers.
4. Migration of protons across the membrane.
5. Water flux across the membrane.
6. Electrochemical reaction with the catalyst domains.
7. Heat transport via conduction and convection within the fuel cell.

These transport properties are determined by using the Maxwell-Stefan equation for multi-component diffusion, the Navier-Stokes equation for momentum transport, the Butler-Volmer and Tafel equations for electrochemical reactions and the Schögl equation for water flux across the membrane.

2.1 Model Assumptions

To reduce computational cost, several assumptions are considered:

1. Operation of the fuel cell is under steady-state conditions.
2. Reactants are compressible ideal gases and are fully saturated with water vapour.
3. Flow in the fuel cell is laminar.
4. The membrane is impermeable to reactant gases.
5. Water produced is assumed to be in liquid phase. Liquid and gas phases have no interaction.
6. The membrane is fully humidified. Ionic conductivity is constant as a result and there is no concentration gradient of water across the membrane.
7. Contact losses between electrical components are not considered in the model.
8. Materials are isotropic and homogenous.
9. Effects of cell compression on the MEA are not considered in this model.

2.2 Governing equations

The flow in the channels is governed by the Navier-Stokes and continuity equations:

$$\rho(\mathbf{u}\cdot\nabla)\mathbf{u} = \nabla\cdot\left[-p\mathbf{I} + \mu\left((\nabla\mathbf{u} + (\nabla\mathbf{u})^T\right) - \frac{2}{3}(\nabla\cdot\mathbf{u})\mathbf{I}\right] \quad (1)$$

$$\nabla\cdot(\rho\mathbf{u}) = 0 \quad (2)$$

where u is the gas velocity (m s^{-1}), ρ is the gas density (kg m^{-3}), p is the pressure (Pa), and μ is the dynamic viscosity of the gas mixture (kg $m^{-1}s^{-1}$).

In the porous gas diffusion catalyst layers, the flow is determined by:

$$\left(\frac{\mu}{\kappa} + Q\right)\mathbf{u} = \nabla\cdot\left[-p\mathbf{I} + \frac{\mu}{\varepsilon}\left(\nabla\mathbf{u} + (\nabla\mathbf{u})^T - \frac{2}{3}(\nabla\cdot\mathbf{u})\mathbf{I}\right)\right] \quad (3)$$

$$\nabla\cdot(\rho\mathbf{u}) = Q \quad (4)$$

where ε is the GDL porosity and κ is the GDL permeability (m^2).

Species mass transport is described by the Maxwell-Stefan equation in the flow channels, gas diffusion layers and the catalyst layers. Hydrogen and water are the species in the anode. Oxygen, nitrogen and water are the species in the cathode. The equation is shown below:

$$\nabla\cdot\left(\omega_i\rho\mathbf{u} - \rho\omega_i\sum_{j=1}^{k}\tilde{D}_{ij}\left(\frac{M}{M_j}\left(\nabla\omega_j + \omega_j\frac{\nabla M}{M}\right) + (x_j - \omega_j)\frac{\nabla p}{p}\right)\right) = R_i \quad (5)$$

$$\rho = \left(\sum_i x_i M\right)\frac{p}{RT} \quad (6)$$

where w is the mass fraction, x is molar fraction, M is the molecular mass (kg mol^{-1}), R is the universal gas constant (8.314 J mol^{-1} K^{-1}), D_{ij} is the binary diffusion coefficient of species i and j (m^2 s^{-1}), and T is the operating temperature of the cell.

R_i is the reaction rate of species i in the catalyst area. The reaction rate for each species are shown below:

$$R_{H_2} = -\frac{M_{H_2}}{2F} i_a \tag{7}$$

$$R_{O_2} = -\frac{M_{O_2}}{4F} i_c \tag{8}$$

$$R_{H_2O} = \frac{M_{H_2O}}{2F} i_c \tag{9}$$

where F is the Faraday's constant (96845 C mol^{-1}).

The current in a PEM fuel cell consists of both electronic and ionic current. Electrons produced at the anode electrode travel through the solid conductive layers of the cell to the cathode electrode where they are consumed in the cathodic reaction. The ionic current is formed from the protons that travel across the membrane. The following charge balances, based on Ohm's law, are used in the model to describe both types of current:

$$\nabla(-\sigma_s \nabla \cdot \phi_s) = S_s \tag{10}$$

$$\nabla(-\sigma_m \nabla \cdot \phi_m) = S_m \tag{11}$$

where σ is the electric conductivity (S m^{-1}), ϕ is the phase potential and S is the current source (A m^{-3}).

The source terms above are governed by the electrochemical reaction:

Anode: $S_m = i_a$ and $S_s = -i_a$ (12)

Cathode: $S_m = i_c$ and $S_s = -i_c$ (13)

The electrochemical reactions in the catalyst layers involve the production or consumption of species in order to produce the electronic current. A linear form of the Butler-Volmer is used to determine the current at the anode due to the fast kinetics of the anode reaction. The cathode reaction, which generally has slow reaction kinetics, is given by the Tafel equation:

$$i_a = a i_{0,a}^{ref} \left(\frac{C_{H_2}}{C_{H_2,ref}} \right)^{0.5} \left(\frac{\alpha_a + \alpha_c}{RT} F\eta \right) \tag{14}$$

$$i_c = -a i_{0,c}^{ref} \left(\frac{C_{O_2}}{C_{O_2,ref}} \right) \exp\left(-\frac{\alpha_c}{RT} F\eta \right) \tag{15}$$

Heat transport by conduction and convection is given by the equation below:

$$\rho c_p u \cdot \nabla T = \nabla \cdot (k \nabla T) + Q \tag{16}$$

where c_p is the specific heat capacity of the fluid (J kg^{-1} K^{-1}) and k is the thermal conductivity (W m^{-1} K^{-1}).

The heat source, Q, is the sum of the heat generated from the electrochemical reactions, activation energy loss and heating within the components due to resistance. The reaction heat generated at the anode is small in comparison to that of the cathode, and is considered negligible in this model. The heat generated at the cathode is determined by:

$$Q_c = \left(\frac{T(-\Delta S_c)}{4F} + \eta_{act} \right) i_c \tag{17}$$

A similar approach to Berning et. al. is used to evaluate the flux of water across the membrane [1]. The Schögl equation is used to account for the water flux across the membrane:

$$u_{w,m} = \frac{k_\phi}{\mu_w} z_f c_f F \cdot \nabla\Phi - \frac{k_p}{\mu_w} \cdot \nabla p \tag{18}$$

where $u_{w,m}$ is the velocity of water across the membrane, k_ϕ is the electrokinetic permeability (m^2), μ_w is the dynamic viscosity of water (kg m^{-1} s^{-1}), z_f is the fixed-site charge, c_f is the concentration of fixed sites and k_p is the hydraulic permeability (m^2).

Inlet velocities were calculated based on stoichiometric ratio, the cell active area, the inlet pressure and cross-sectional area. Initial conditions for the model also include atmospheric pressure at the channel outlets and inlet mass fractions of the gas species. The initial cell temperature is 80 °C. The anode potential is 0 V and the cathode potential is the operating cell potential. Model constants were obtained from literature [1,6,7].

3. Solution procedure

COMSOL Multiphysics 4.2 was used to solve the model for each flow field. Structured meshes were created for each in order to minimize computational cost while providing a

sufficient degree of accuracy. A mesh sensitivity analysis was conducted to ensure this condition was met. The model was solved using a MUMPS solver. Each run of the solver had a computational time of approximately 3715 s to solve the model across a range of voltages from 0.5 V to 0.9 V. The results of the model for each flow field design were validated against similar results in literature and were found in good agreement with the overall transport characteristics [1, 7].

4. Results

Figure 3 shows the polarization curves of the PEMFC fuel with each flow field plate design. The fuel cell shows nearly identical performance in terms of the current density at a given voltage for both the parallel and circular channel designs. The performance of the cell with the circular design is fractionally lower than that of the parallel design at higher current densities.

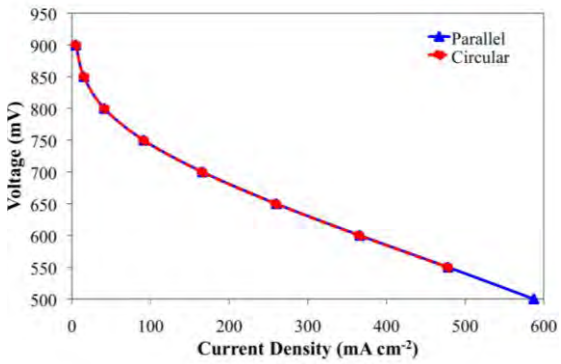

Figure 3. Polarization curves of the PEM fuel cell with parallel and circular flow fields.

Modelling mass transport within the cell gives a detailed distribution of species within the different layers. For both flow field designs at 0.6 V, it is evident that species concentration decreases along the flow in the x direction as shown in Figures 4-7. Depletion of hydrogen in the anode catalyst layer and oxygen in the cathode catalyst layer has a non-uniform distribution within both designs. The consumption of reactant species in both electrodes is significantly higher under the rib of the PCB than under the channel areas as seen in Figures 8 and 9. Specifically, the depletion of oxygen is strong under the rib of the circular design. The current collector restricts the transport of species within this area. As a result, mass transport limitations contribute to a loss of cell performance. Furthermore, water management is a potential issue as product water may not be removed quickly enough and could flood the areas under the rib with prolonged operation. The parallel flow design shows a more uniform distribution of oxygen along the cathode-membrane interface.

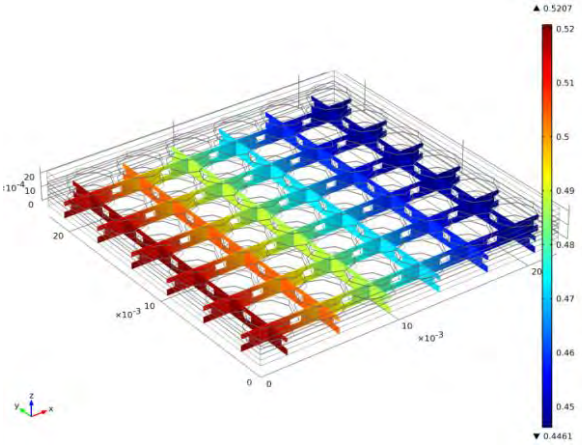

Figure 4. Mass fraction of hydrogen on the anode side at 0.6 V in the circular flow field design. Hydrogen flow is in the *x* direction.

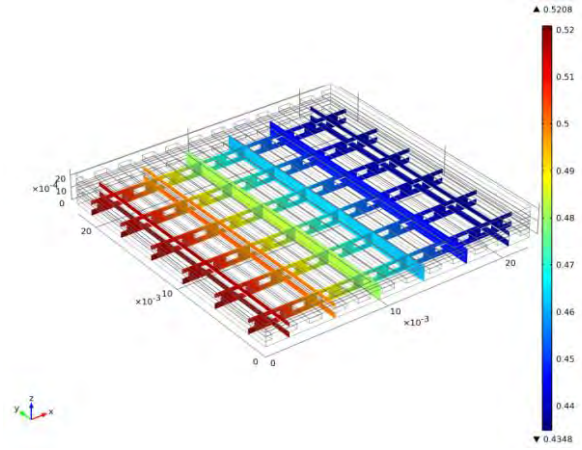

Figure 5. Mass fraction of hydrogen on the anode side at 0.6 V in the parallel flow field design.

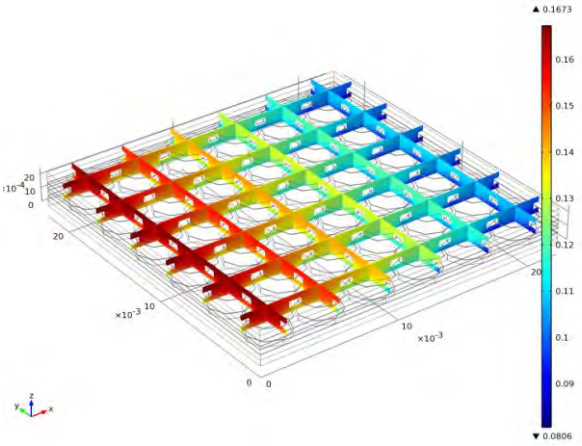

Figure 6. Mass fraction of oxygen on the cathode side at 0.6 V in the circular flow field design.

Oxygen decreases with flow along the *x* direction due to reaction consumption in the catalyst layer.

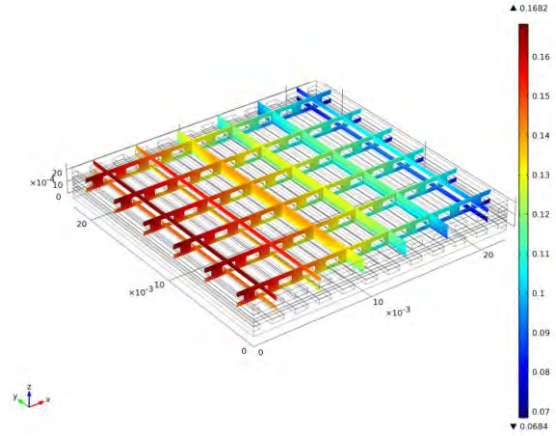

Figure 7. Mass fraction of oxygen on the cathode side at 0.6 V in the parallel flow field design.

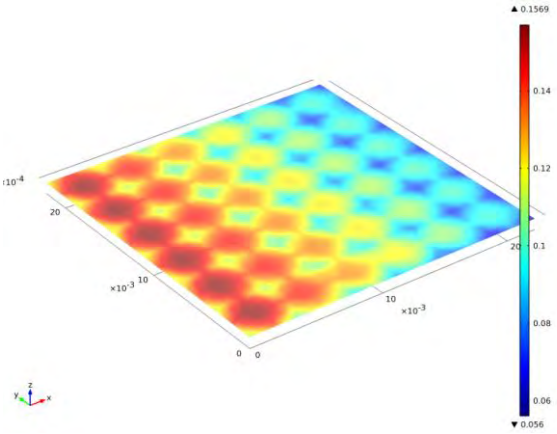

Figure 8. Mass fraction of oxygen at the cathode-membrane interface at 0.6 V in the circular flow field design. Lower mass fractions can be seen in areas under the ribs.

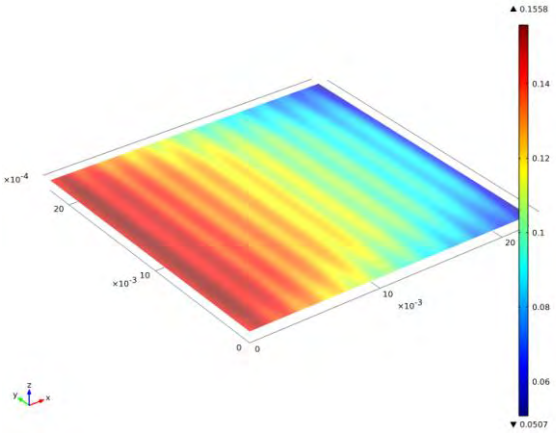

Figure 9. Mass fraction of oxygen at the cathode-membrane interface at 0.6 V in the parallel flow field design. A more uniform oxygen distribution can be seen in comparison to that in Figure 8.

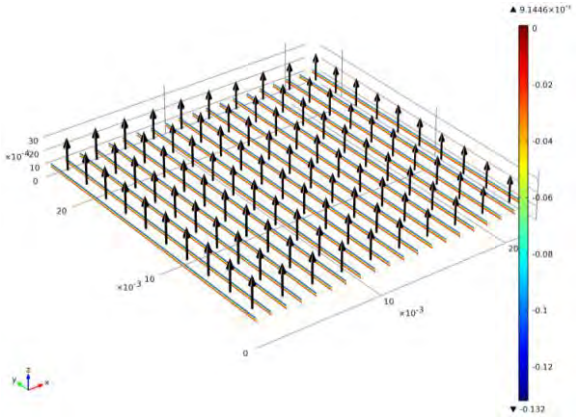

Figure 10. Water flux across the membrane, represented by the arrows, from the anode to the cathode. Electrolyte potential is also displayed across the membrane.

Figure 10 demonstrates the flux of water across the membrane at 0.6 V. At this potential, the electro-osmotic drag term of the Schögl equation is greater than the pressure term, which results in a total flux of water from the anode to the cathode. The membrane is assumed to be fully humidified; no back diffusion of water to the anode occurs. Consequently, the current collectors presented would need modification to allow for a balance between sufficient humidification and removal of excess water in the fuel cell.

In addition to mass transport, heat transport within the cell is an important consideration when selecting a flow field plate design. The temperature distribution within the cell affects current, mass and momentum transport so understanding it fully can prevent failure during operation of the fuel cell. Figures 11 and 12 show the temperature distribution within the cell. The temperature of the fuel cell

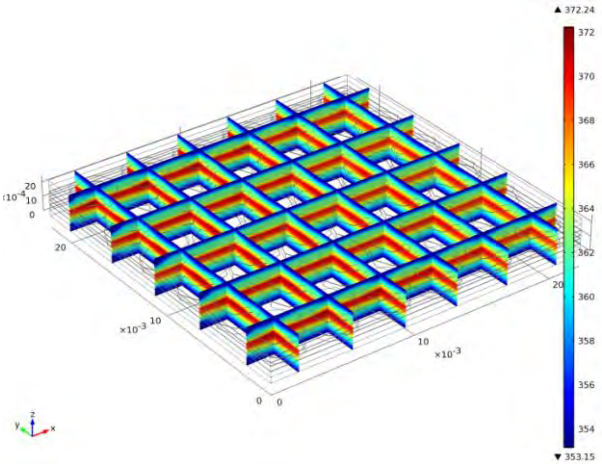

Figure 11. Temperature distribution in the fuel cell with a circular channel plate design.

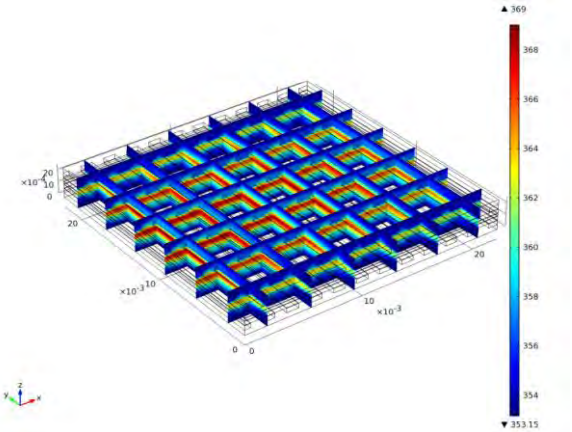

Figure 12. Temperature distribution in the fuel cell with a parallel channel plate design.

with each design is greatest in the membrane due to its lower ionic conductivity and in the cathode catalyst layer due to the electrochemical reaction. The temperature rises in the configuration with the circular channels from 353 K to 372 K. This is slightly higher than that of the configuration with the parallel channels at 353 K to 369 K. However, Figure 11 shows that a greater proportion of the MEA operates at higher temperatures in comparison to that of Figure 12. Operating at higher sustained temperatures can result in insufficient humidification within the membrane, which results in lower ionic conductivity. Furthermore, increased temperatures can result in structural deformation of the cell components. Although phase change is not considered here, the production of liquid water in the fuel would have a cooling effect. Excess heat generated at the cathode would cause evaporation of the liquid water resulting in a local decrease in temperature. Hence, overall temperature rise in the fuel cell would be lower than that predicted by the model presented here.

The model for each design indicates that operating the fuel cell with a gas plenum region possibly contributes to decreased cell performance. The gases transported to the cell in the channels have a velocity of approximately an order of magnitude lower compared to the inlet velocity. This limits effective transport of reactants, products and heat resulting in limiting current densities at higher voltages. In order to overcome this challenge, design and operating parameters need further optimization.

5. Conclusions

A detailed model of a PEM fuel cell was solved to investigate the effect of flow field design on mass, charge, momentum, heat and water transport. Even though the circular and parallel flow field plates exhibited similar cell performance in terms of the polarization curve, the parallel design shows more potential for use in a fuel cell. When operating with this design, the fuel cell demonstrated more uniform distributions of both mass and heat within the various layers, which is key for successful long-term performance. Further work is currently being undertaken to investigate various design improvements, fuel cell operation with variations in membrane humidification and the inclusion of phase change.

6. References

1. Berning, T., Lu, D.M., Djilali, N., Three-dimensional computational analysis of transport phenomena in a PEM fuel cell, *J. Power Sources*, **106**, 284-294 (2002)

2. Djilali, N., Lu, D.M., Influence of heat transfer on gas and water transport in fuel cells, *Int. J. Thermal Sciences*, **41**, 29-40 (2002)

3. Fuller, T.F., Newman, J., Water and Thermal Management in Solid-Polymer-Electrolyte Fuel Cells, *J. Electrochem. Soc.*, **140**, 1218-1225 (1993)

4. Gurau, V., Liu, H., Kakac, S., Two-Dimensional Model for Proton Exchange Membrane Fuel Cells, *AIChE Journal*, **44**, 2410-2422 (1998)

5. Nyugen, T.V., White, R.E., A Water and Heat Management Model for Proton-Exchange-Membrane Fuel Cells, *J. Electrochem. Soc.*, **140**, 2178-2186 (1993)

6. Um, S., Wang, C.Y., Chen, K.S., Computational Fluid Dynamics Modelling of Proton Exchange Membrane Fuel Cells, *J. Electrochem. Soc.*, **147**, 4485-4493 (2000)

7. Wöhr, M., Bolwin, K., Schnurnberger, W., Fischer, M., Neubrand, W., Eigenberger, G., Dynamic Modelling and Simulation of a Polymer Membrane Fuel Cell Including Mass Transport Limitation, *Int. J. Hydrogen Energy*, **23**, 213-218 (1998)

8. Ziegler, C., Tranitz, M., Schumacher, J.O., *A model for planar self-breathing proton exchange membrane fuel cells in FEMLAB*, Oral presentation, Published in: Proceedings of

the COMSOL Multiphysics User's Conference, Frankfurt, Germany (2005)